ELSEVIER

Physics of the Earth and Planetary Interiors 86 (1994) 263–276

PHYSICS
OF THE EARTH
AND PLANETARY
INTERIORS

Anisotropy and the splitting of PS waves

Liqiang Su *, Jeffrey Park

Department of Geology and Geophysics, Yale University, New Haven, CT 06511, USA

Received 18 October 1993; revision accepted 30 March 1994

Abstract

The PS wave is radially polarized in an isotropic spherically symmetric Earth owing to the P to SV conversion at the free surface. If we choose stations with weak SKS splitting to minimize the effect of the receiver, we can measure the anisotropy beneath the bounce point of the PS wave. We find that with a deep source and epicentral range of $90° < \Delta < 125°$, the PS phase can be distinguished from other phases. Owing to the limitation of recent large deep events with epicentral range between 90° and 125°, we analyze data from stations in North America and events beneath the Bonin Islands and the Fiji Islands. For events in these two regions, the bounce points of the PS wave are roughly located northwest of the Kuril Islands and near the Nova–Canton Trough in the central Pacific, respectively. Because the first Fresnel zone for the PS wave at this distance range is roughly 700 km across, each PS splitting observation must be interpreted as a local average of anisotropic properties. The average direction of the fast axis of anisotropy below the Nova–Canton Trough region is N104.2°E with a standard deviation 12.7° and a typical delay time of 1.8 s. Landward of the Kuril Islands, the average direction of the fast axis is N127.6°E clockwise from north, and the standard deviation is 11.3°, with a typical delay time of 1.2 s. We have compared the fast axis with the direction of fossil seafloor spreading and with the present-day absolute plate motion. The fast axis of anisotropy at the Nova–Canton Trough agrees well with the direction of absolute plate motion, and poorly with the complex fossil spreading pattern. This suggests that significant upper-mantle shear anisotropy exists in this part of the central Pacific, and is consistent with mineral alignment owing to strain associated with present-day plate motion. Similarly, the fast axis beneath the Kuril Islands parallels the convergent motion of the slab. Coupled-mode synthetics constructed with the 'strong' Born approximation can be used to model the interaction of the PS waves with anisotropic structure that has a horizontal axis of symmetry. We use all free oscillations up to 35 mHz in the calculation. The coupled-mode synthetics show shear-wave splitting with delay time and fast axis consistent with the ray theory prediction.

1. Introduction

Anisotropy has a close relation to the strain-induced lattice preferred orientation of highly anisotropic crystals such as olivine and orthopyroxene (Nicolas and Christensen, 1987; Ribe, 1989a,b; Ribe and Yu, 1991). Measurement of anisotropy has become an important means of studying motions in the mantle associated with plate tectonics. Azimuthal anisotropy was initially observed for Pn velocities measured in marine seismic refraction studies (Hess, 1964; Raitt et

* Corresponding author.

SSDI 0031-9201(94)02949-C

al., 1969; Keen and Barrett, 1971). It strongly suggests that the anisotropy in the oceanic crust and sub-Moho mantle is due to fossil fabric formed at the spreading ridge. Anisotropy inferred from long-period surface waves (Forsyth, 1975; Nataf et al., 1984; Tanimoto and Anderson, 1985; Montagner and Tanimoto, 1990) suggests that the fast axis of anisotropy is consistent with the present-day flow direction of kinematic plate models.

Keith and Crampin (1977) indicated that shear waves suffer splitting in anisotropic structures because the incident shear wave separates into two orthogonal polarizations travelling with different velocities. The polarization direction and the delay time between two arrivals can constrain the fast direction of anisotropy. Ando and Ishikawa (1982) investigated the anisotropy in the upper mantle beneath Honshu by measuring the splitting of ScS phases from nearby events in the descending slab. The SKS phase has been widely used to measure the anisotropy beneath seismic stations because of its simple radial polarization and its easy identification if the epicentral distance is larger than 85°). The SKS splitting method, first introduced by Vinnik et al. (1984), has been systematically discussed by Kind et al. (1985); Silver and Chan (1988, 1991); Vinnik et al. (1989) and Savage et al. (1990).

The sparse distribution of stations and distribution of seismicity at plate boundaries make large areas, such as the central Pacific, inaccessible to SKS splitting measurements. Complementary information on lateral gradients of anisotropy can be obtained from long-period quasi-Love scattered phases (Park and Yu, 1993; Yu and Park, 1994), and remote regions can be sampled with the bounce points of other body phases. Recently, Fischer and Yang (1994) have used S–sS pairs to investigate the Kuril Islands region where no stations are near. In this paper, we choose the PS phase to analyze. The PS phase consists of a P wave that converts to an S wave at the free surface. Thus, the PS waveform is sensitive to mantle properties beneath its bounce point. Like the SKS phase, the PS phase is radially polarized in an isotropic, spherically symmetric Earth. In the absence of intense scattering or strong off-azimuth refraction, significant energy of the PS phase on the transverse component suggests the existence of anisotropy.

This paper demonstrates the feasibility of using the PS phase for the investigation of mantle anisotropy. We restrict the data set to source–receiver pairs where PS splitting appears clear and can be related confidently to mantle properties near its bounce point. In the larger global data set, PS splitting observations can be used to investigate bounce-point properties after the effects of structure beneath the receiver have been subtracted. We also report numerical simulations of shear-wave splitting of long-period body waves in simple anisotropic spherical Earth models. The ability to model such effects is useful when establishing 'ground truth' for shear-wave splitting interpretations. To this end, we use synthetic seismograms from coupled free oscillations using the strong Born approximation (Su et al., 1993) and coupling formulae derived by Park and Yu (1992) and Yu and Park (1993) for simple anisotropic Earth models.

2. Method

To detect and measure PS splitting, we need to separate it from the SP phase and from other body waves. For a hypocenter at the Earth surface, the PS and SP phases arrive simultaneously. However, if a hypocenter is deep, the PS and SP waves can be separated because the shorter S wave path of the SP phase causes it to arrive earlier than the PS phase. The deeper the hypocenter, the larger the gap between the PS and SP phases. At epicentral distances $60° \leqslant \Delta \leqslant 85°$, the long-period PS and S phases arrive closely in time, making separation difficult. If $\Delta > 125°$, it is difficult to separate the PS wave from other phases such as PKKP, ScSP and SKSP on long-period seismograms. Based on this, we chose a data set with $90° \leqslant \Delta \leqslant 125°$ in this study.

Previous studies (e.g. Vinnik et al., 1984; Silver and Chan, 1988) have shown that a shear wave will split when it travels through an anisotropic structure. Olivine is thought to be the major cause of upper-mantle anisotropy, but it is unstable deeper than 420 km; its anisotropy can contribute only within the uppermost mantle and crust. There are three possible regions which can generate PS splitting. The upper mantle and crust beneath the receiver, the source or the PS wave bounce point are anisotropic. Crustal anisotropy is a poor candidate to explain relative splitting delays $\delta t \gtrsim 1$ s, because, for reasonable mineral assemblages, it is too thin, especially for oceanic crust. Anisotropy between the D″ layer and the 420 km olivine–spinel transition has been found negligible in SKS splitting studies (Kaneshima and Silver, 1992; Silver et al., 1993). Because we selected only deep events, the source region should not affect the PS phase.

Fig. 1 is a typical PS raypath, in real scale, with the epicentral distance of 110° and the source at 450 km. The greater part of the S leg of the PS raypath is in the lower mantle except near the bounce point and receiver. The incidence angle of the S ray segment at the 670 km discontinuity is 28.1°. The remaining problem is how we determine whether anisotropic structure exists beneath the receiver or the bounce point or both. Measurements of SKS splitting have been widely used to detect the anisotropic structure beneath both fixed and portable seismic stations (Silver and Chan, 1991; Savage and Silver, 1993). To meet our purpose in this paper, we chose those stations where SKS splitting is small ($\delta t \lesssim 0.5$ s). We infer that there is an anisotropic structure beneath the bounce point if PS splitting is much larger than that of SKS.

To verify this working hypothesis, we performed a comparison of synthetic seismograms calculated with coupled free oscillations with spherical-Earth synthetics. We use a model with a zonal anisotropic belt around the Earth's equator. We compare synthetics from two source–receiver pairs. For the first source–receiver pair, the receiver is outside the anisotropic zone, and the PS bounce point is within the anisotropic belt. In the second case, the receiver is in the anisotropic belt. In this calculation, we used the 'strong' Born coupling approximation (Su et al., 1993) using all normal modes having degenerate frequency $f < 35$ mHz. The spherical-Earth reference model used is oceanic preliminary Earth model (PEM) of Dziewonski et al. (1975). Because the asphericity is zonal, the coupling interaction is restricted to free-oscillation singlets with equal azimuthal order m (Park and Yu, 1992), which greatly simplifies the numerical calculation. We prescribe a coupling halfwidth Δf so that two normal modes with spherical-Earth frequencies f_1, f_2 interact only if the frequency difference

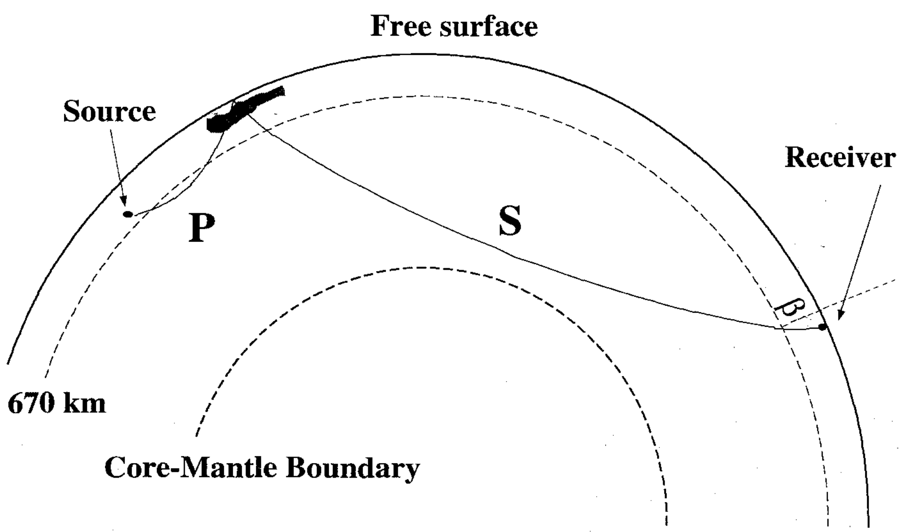

Fig. 1. A raypath for a PS wave in the PEM model. In this case, the epicentral distance is 110°, and the source depth is 450 km. The incidence angle β through the 670 km discontinuity is 28.1°. The shaded area represents the anisotropic structure.

$|f_1 - f_2| \leqslant \Delta f$. We choose $\Delta f = 0.25$ mHz. Although the 35 mHz cutoff frequency is not high enough to model a typical broadband PS phase, the seismogram should exhibit shear-wave splitting related to the real data. The synthetic particle motions are convolved with a typical broadband instrument response with sample rate of 1 s.

Fig. 2 shows the spherical-Earth and coupled-mode synthetics for the first source–receiver pair. A PS waveform anomaly on the transverse component of the coupled-mode synthetics is obvious, whereas for the SKS phase no such anomaly is seen on the transverse component. The particle motion of the PS phase becomes slightly elliptical, as well as slightly off-azimuth. The ellipticity of the wave is weak, however, as it represents a 1–2 s splitting delay in a body wave with period $T \gtrsim 30$ s. If the same time delay were imposed on a PS phase with a dominant period of 10 s, the ellipticity would be much greater.

In the case where the receiver region is anisotropic, we can see an anomaly associated

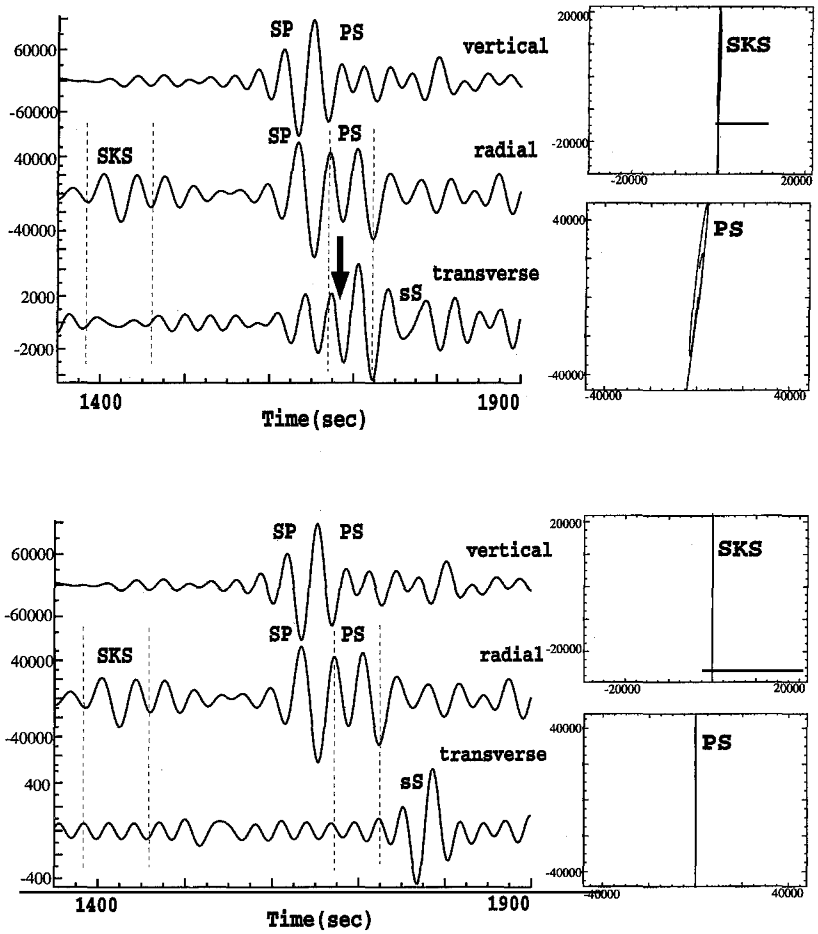

Fig. 2. Comparison of spherical-Earth synthetics and coupled-mode synthetics. The anisotropic model is a zonally symmetric belt (latitude −25° to 25°) at the Earth's equator with east–west anisotropic orientation. The thickness of the anisotropic model is 400 km, and the epicentral depth is 600 km. The locations of the receiver and the epicenter are chosen as (69.7°W, 58.33°N) and (13.76°E, 30.07°S), respectively, so that the PS wave bounces in the anisotropic structure at the equator. The plots of particle motion for the SKS and PS phases are on the right side. Upper panel: three-component coupled-mode synthetics. Lower panel: three-component synthetics for a spherical Earth. The transverse component of the coupled-mode synthetics shows a significant anomaly at the time of the PS arrival.

with SKS, PS, PPS, etc. on the transverse component (Fig. 3). The ellipticity of the PS phase is stronger in this example.

We use coupled-mode synthetics to measure the fast velocity direction which we have specified in our model. If there is no anisotropic structure along the raypath, the transverse component should be identically zero for P–SV polarized phases, such as SKS, SKKS, PS and PPS. When an anisotropic structure is specified, the shear wave splits, and particle motion in the horizontal plane will be partly elliptical. One polarization travels with faster velocity and the other with slower velocity. Thus, at the receiver, these two phases combine on the radial and transverse components with a first-order time delay $\delta t \approx (h/\bar{\beta})(\delta\beta/\bar{\beta})$, where $\bar{\beta}$ is the average S velocity in an anisotropic layer, h is the layer's thickness, and $\delta\beta/\bar{\beta}$ is the fractional change in shear velocity associated with the anisotropy, assumed to be azimuthal. If we rotate radial and transverse components an angle α to the fast direction, we should obtain identical waveforms that have travelled with faster and slower velocity. If such 'pure' signals are found, we find the time shift δt which aligns the phases on the horizontal components.

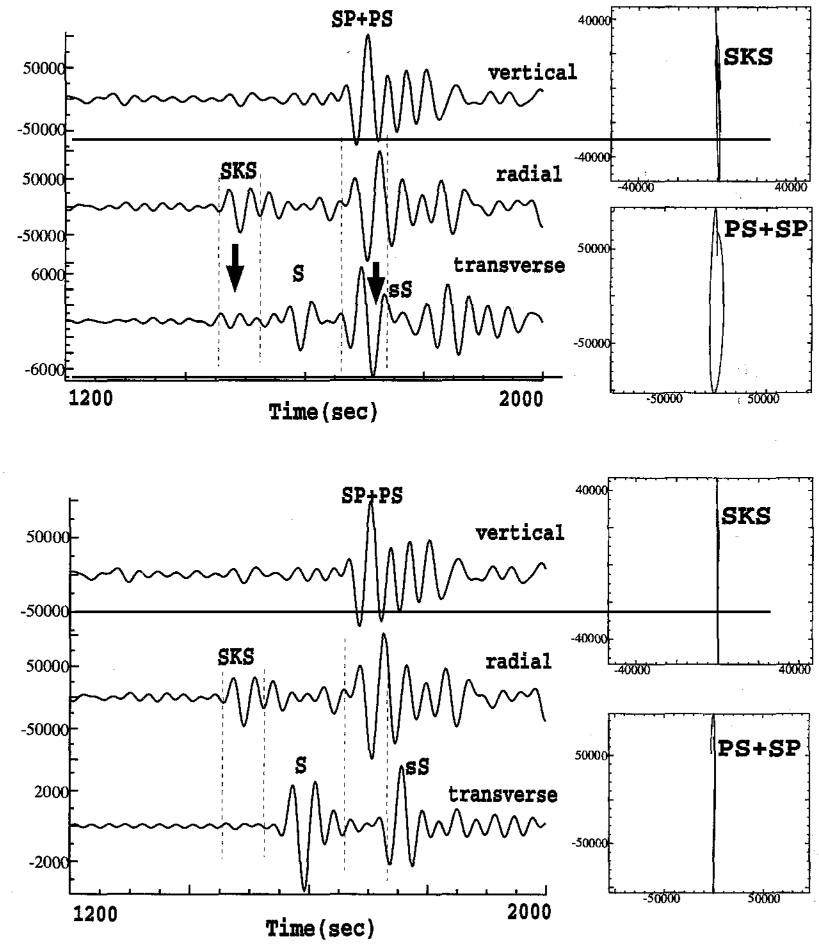

Fig. 3. Same anisotropic model as in Fig. 2. We set the location of the receiver at (105.0°E, 15.0°S) and the epicenter at (0.0°E, 70.0°N). Thus, the receiver lies in the anisotropic zone, and the anisotropic structure below the receiver will generate shear-wave splitting. We show the coupled-mode synthetics at the upper panel and the spherical-Earth synthetics at the lower panel. The anomalies of the SKS and PS phases on the transverse component of the coupled-mode synthetics are clear.

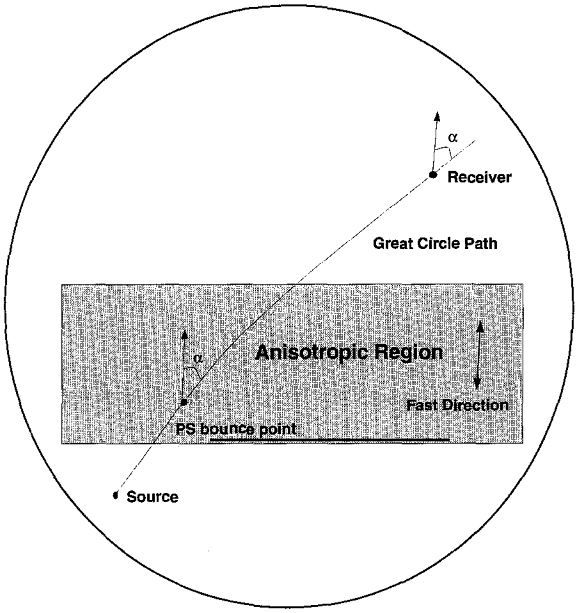

Fig. 4. Scheme to illustrate the relationship between fast phase orientation at the receiver and fast anisotropic orientation at the PS-wave bounce point.

As the faster signal has a phase advance relative to the slower one, we shift the signals with a predicted time δt. After we rotate back to the radial and transverse direction, the signal on the corrected transverse component should be absent. In practice, we use the technique of Silver and Chan (1988) to minimize the 'energy' on the corrected transverse component in a search over all plausible angles α and delays δt. Then we project back to the bounce point, changing the sign of the radial component to account for the ray caustic (Fig. 4).

In a synthetic test, six paths with different source azimuths are used. The average direction has strike 82.7° clockwise from north (the correct value is 90°) and the measurements scatter with standard deviation 11.5°. The scatter in the measurements might be caused by long-period S-to-P energy conversion which is neglected by the ray-based SKS shear-wave splitting model. Alternatively, we may suffer limited precision when measuring the small perturbation to a 30 s body wave caused by a 1–2 s splitting delay. The PS wave, unlike the nearly vertical SKS raypath through the mantle, has a larger incidence angle that varies along the path. Strictly, the S wave of the PS phase will split along every infinitesimal path segment through the anisotropic region. The Silver and Chan (1988) interpretation is based on the assumption that the vertical-incidence splitting in a single layer can represent the total integrated splitting.

3. Observations

We have considered events deeper than 450 km with $m_b > 5.5$ (Table 1). Our data sources include the Global Digital Seismographic Network (GDSN), Regional Seismic Telemeter Network (RSTN) and Global Seismic Network (GSN). Fig. 5(a) shows data for Event 86167 (a 16 June

Table 1
Earthquake events used in the study

Event	Latitude	Longitude	Depth (km)	m_b	Location
85359	21.56°S	178.72°W	481.7	5.6	Fiji Islands region
86034	27.89°N	139.40°E	515.7	5.7	Bonin Islands region
86051	22.01°S	179.64°W	600.8	5.6	South of Fiji Islands
86076	27.36°N	139.83°E	499.7	5.5	Bonin Islands region
86091	17.91°S	178.63°W	541.0	5.7	Fiji Islands region
86146	7.07°S	124.19°E	553.2	6.8	South of Fiji Islands
86167	21.90°S	179.04°W	565.2	6.1	Fiji Islands region
86183	21.95°S	179.66°W	597.4	5.5	Fiji Islands region
93080	17.70°S	178.80°W	590.0	6.3	Fiji Islands region
93106	17.40°S	178.90°W	569.0	5.9	Fiji Islands region

The data of 1985 and 1986 are from the NEIC. The data of 1993 are from the Incorporated Research Institutions for Seismology (IRIS) Data Management Center.

1986 earthquake beneath the Fiji Islands, $m_b = 6.1$) recorded at RSSD. (The National Earthquake Information Center (NEIC) hypocentral depth is 562.2 km.) We can easily identify the SKS, SP and PS phases on the vertical and radial components. At the time of the PS arrival, the anomaly on the transverse component is obvious. Fig. 5(b) illustrates that the horizontal particle motion is elliptical for the PS phase. Furthermore, when we rotate radial and transverse components to 35° clockwise from north, Fig. 5(c) clearly shows that the PS phase has split into two signals. However, at the time of SKS phase arrival, it is difficult to find an amplitude anomaly on the transverse component. This implies that the cause of the PS splitting is the anisotropic structure beneath the PS bounce point, not the structure below the receiver. Silver and Chan (1991) measured a fairly small SKS delay time $\delta t \approx 0.65$ s at RSSD. Our observation also suggests that the splitting effect is weak beneath RSSD. Fig. 6 is the contour plot of corrected transverse component energy $E(\delta t, \alpha)$ for the SKS phase and PS phase, where δt is the delay time related to anisotropy and α is the angle of the fast direction counter-clockwise from radial

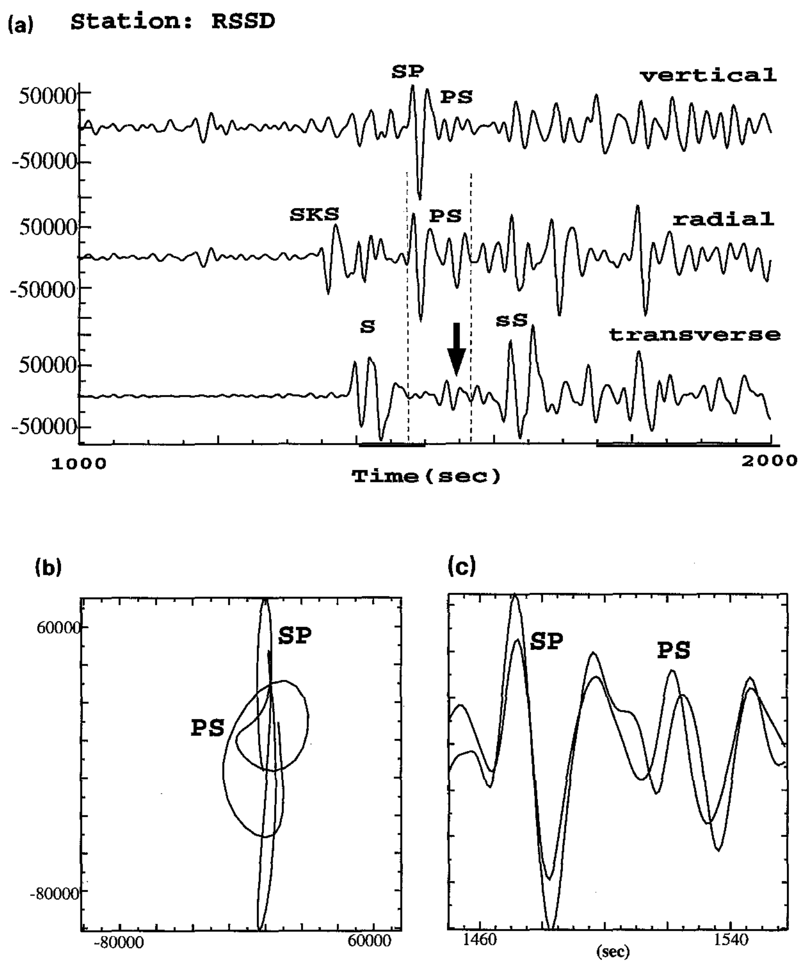

Fig. 5. (a) Three-component data at Station RSSD for the 16 June 1986 Fiji event ($m_b = 6.1$). The data are lowpassed at 0.1 Hz. The dashed line indicates the time window selected for analysis. (b) Horizontal particle motion in the selected time window, referenced to seismometer axes. (c) Seismograms of the two horizontal components, rotated to align with the inferred 'fast' and 'slow' propagation axes.

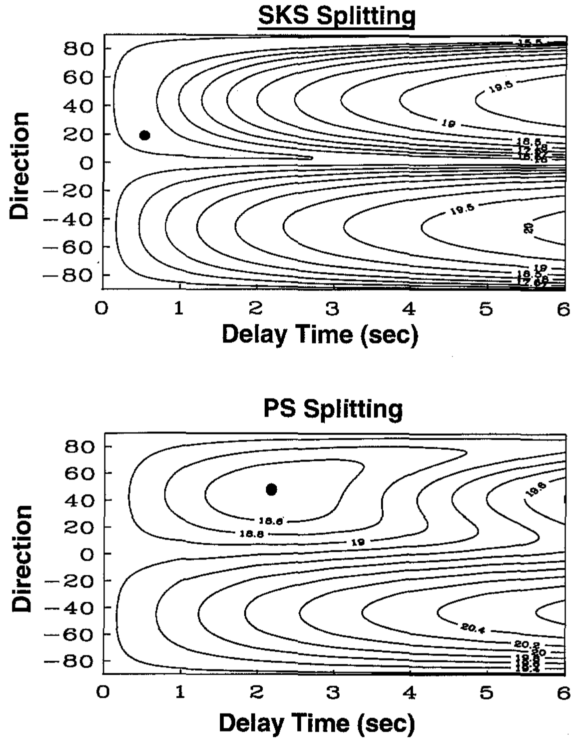

Fig. 6. Contour plots of energy on the corrected transverse component for the SKS and PS phases. α is defined as the angle clockwise from the radial component. The contour value on the plots is logarithmic. (a) SKS phase: $\delta t = 0.5$ s and $\alpha = 20°$. In geographical coordinates this corresponds to N64.3°E. (b) PS phase: $\delta t = 2.1$ s and $\alpha = 50°$. In geographical coordinates this corresponds to N100.9°E at the PS bounce point.

component. Fig. 7 and Fig. 8 show two other examples of seismograms from deep Fiji events 86183 (2 July 1986, $m_b = 5.5$) and 93080 (21 March 1993, $m_b = 6.3$) recorded at RSNY and HRV, respectively. On the transverse components, as with Fig. 5(a), there are splitting anomalies in the PS wave arrival.

Many of the recent large events deeper than 450 km are located in two regions: the Fiji–Tonga region and the Bonin Islands region. Although some deep events in the Banda Sea and South America regions are available, we did not use these data because there were few stations which have both suitable epicentral distance and weak SKS splitting. In this pilot study we concentrate on the stations in North America, such as LON, RSCP, RSSD, ANMO, CCM, HRV, and SCP. We report one bounce point from Fiji to ZOBO, a South American station, but timing problems at this station greatly restrict the number of usable records.

To calculate the location of the PS bounce point, we use a ray tracing method in a spherical Earth with the oceanic PEM model. For the PS wave, the travel distance of the P segment is much shorter than that of the S segment. Thus, although the stations in North America may be separated by more than 1000 km, the bounce points of the PS wave are clustered for a single source region. The bounce points cluster in the Nova–Canton Trough region in the central Pacific for sources in the Fiji–Tonga region and stations in North America (Fig. 9). For Bonin Islands events, the bounce points cluster northwest of the Kuril Islands. PS splitting measurements are coherent for both clusters, suggesting that this phase offers a stable measurement of integrated anisotropy.

4. Results and conclusion

The lateral resolution of PS splitting measurements depends on the width of the Fresnel zone at the free surface bounce point where P converts to S (Eaton et al., 1991). To estimate the range of raypaths that contribute to the PS observations, we fix the source and receiver location, then perturb the bounce point position. If the travel time difference between perturbed and unperturbed PS raypaths is smaller than $T/4$, where T is the period of the wave, the perturbed bounce point is within the first Fresnel zone. Fig. 10 is a schematic diagram of the first Fresnel zone of the PS phase. Approximately, the first Fresnel zone of PS phase can be thought as an ellipse if we assume $\epsilon^- \approx \epsilon^+$. More roughly, it can be treated as a circle. In this study, a rough approach is enough to estimate the lateral average implicit in the PS observations. For a typical case in this study, with an epicentral distance of 110°, a source at 450 km, and a period of 17 s (frequency 60 mHz), the radius of the first Fresnel zone is about 3.3°. Thus, the measurements reflect an

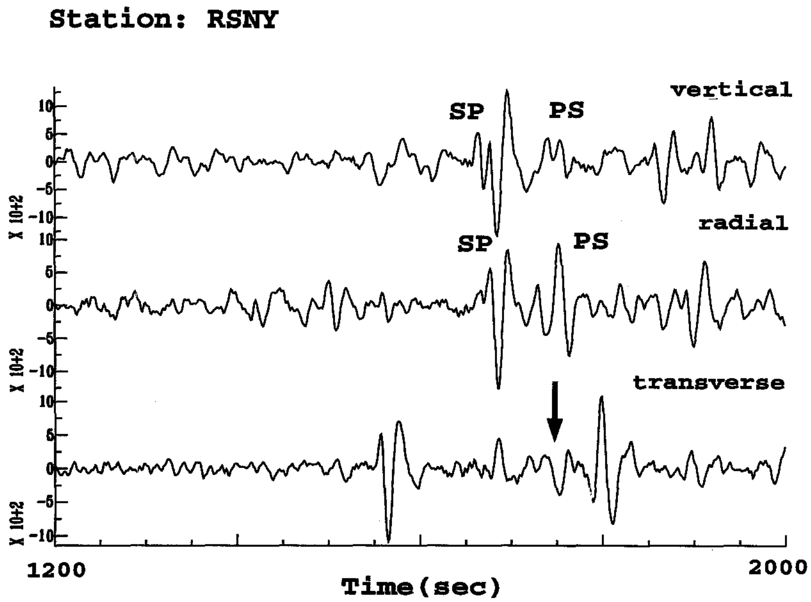

Fig. 7. Three-component data at Station RSNY for the 2 July 1986 Fiji event ($m_b = 5.5$). Unfiltered data are shown.

average of azimuthal anisotropy over a roughly circular region of radius 350 km, rather than beneath a single bounce point.

At the Nova–Canton Trough, the averaged fast direction of azimuthal anisotropy is N104.2°E (clockwise from north). The standard deviation of the data set is 12.7° about the mean. At the Kuril Islands, the averaged fast direction is N127.6°E,

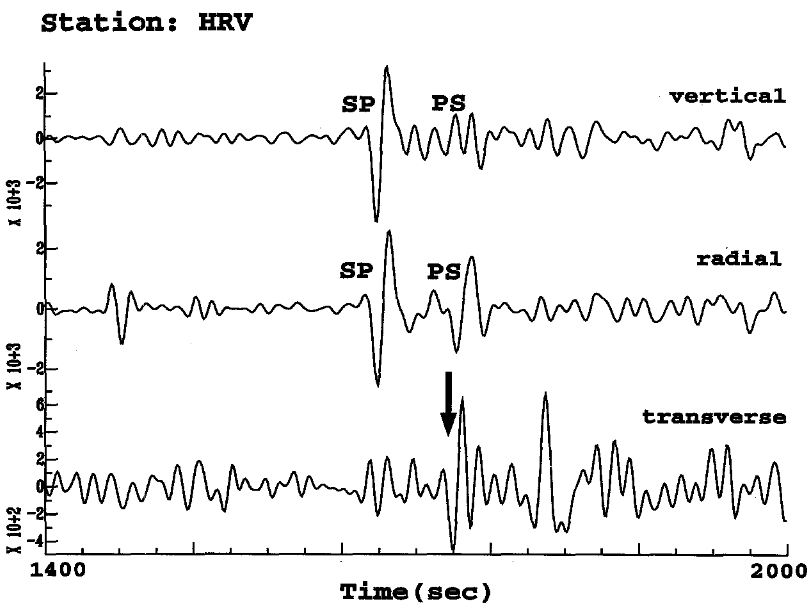

Fig. 8. Three-component data at Station HRV for the 21 March 1993 Fiji event ($m_b = 6.3$). The data are bandpassed between 0.008 and 0.1 Hz.

and the standard deviation of the data set is 11.3° about the mean. Although we plot the PS-wave bounce points on the map as discrete positions, the measurements are the averages along the raypath through the anisotropic region, and are influenced by all rays in the first Fresnel zone. Thus, the average of measurements in a region may be a proper interpretation for the anisotropic structure.

Relative to SKS splitting, the delay time of the PS wave has more uncertainty when determining the strength of anisotropy. This is because the delay time of the PS wave is more sensitive to the epicentral distance. Thus, it is more involved to use delay time of PS-wave splitting to represent the strength of anisotropy quantitatively. However, the much larger delay time of PS-wave splitting still indicates qualitatively the strength of anisotropy at the bounce points of the PS waves. As the delay time δt constrains the product of the anisotropy and the path length, a thicker anisotropic layer would imply weaker anisotropy. If we assume the thickness of the anisotropy is 200 km and the incidence angle through the 200 km layer is about 20°, the average delay time, 1.8 s, near the Nova–Canton Trough leads to 3.65% peak-to-peak shear anisotropy. Northwest of the Kuril Islands, an average delay time of 1.2 s suggests 2.76% peak-to-peak shear anisotropy. If the anisotropy is down to 420 km (the incidence angle is about 24°), it leads to 1.9% peak-to-peak shear anisotropy in the Nova–Canton Trough region and 1.4% northwest of the Kuril Islands.

The direction of present-day absolute plate

Table 2
List of the measurements; the angle of fast direction is defined as clockwise from the north; δt is the estimated delay time between travel times of the fast and slow shear-wave polarizations

Station	Event	δt (s)	PS bounce	Fast direction	Type of data
RSCP	86167	1.6	163.7°W, 11.5°S	265.8	Long period
GAC	86167	–	162.7°W, 6.6°S	290.3	Long period
RSSD	86167	2.1	167.1°W, 9.3°S	280.9	Long period
BOCO	86167	–	159.7°W, 21.2°S	258.1	Long period
CHTO	86167	–	167.3°E, 16.5°S	116.9	Long period
RSCP	86091	–	163.6°W, 7.5°S	309.0	Long period
GAC	86091	–	164.2°W, 4.0°S	274.3	Long period
RSCP	86146	2.0	166.0°W, 9.7°S	259.0	Long period
RSSD	86146	1.5	170.0°W, 8.3°S	267.9	Long period
ZOBO	86146	2.5	162.9°W, 26.4°S	298.7	Long period
RSNY	86146	2.0	164.2°W, 4.5°S	305.5	Long period
HRV	93080	1.8	162.1°W, 3.3°S	277.6	Broad-band
ANMO	93080	2.0	166.1°W, 8.1°S	252.9	Broad-band
RSCP	86183	1.3	164.1°W, 11.5°S	252.9	Long period
GAC	86183	1.3	163.3°W, 6.7°S	284.3	Long period
RSNY	86183	–	162.9°W, 7.0°S	305.6	Long period
RSON	86183	3.1	168.0°W, 8.0°S	297.5	Long period
RSSD	86076	–	150.3°E, 53.0°N	325.8	Long period
RSCP	86076	0.5	153.8°E, 49.0°N	314.5	Long period
RSNY	86076	1.5	146.9°E, 50.6°N	298.2	Long period
RSCP	86051	2.0	163.0°W, 10.9°S	290.7	Long period
RSCP	86034	1.0	153.0°E, 48.7°N	313.1	Long period
SCP	86034	0.8	150.°E, 47.7°N	304.3	Long period
RSNY	86034	2.0	148.4°E, 47.4°N	295.1	Long period
TOL	86034	–	127.9°E, 46.7°N	227.2	Long period
GAC	85359	1.3	167.4°W, 11.2°S	303.0	Long period
RSNT	85359	1.5	172.6°W, 8.2°S	283.2	Long period
RSON	85359	1.6	167.4°W, 7.9°S	299.4	Long period
CCM	93106	1.2	166.9°W, 8.0°S	300.1	Broad-band
HRV	93105	1.2	161.6°W, 2.5°S	275.5	Broad-band

motion is very similar to that of fossil seafloor spreading in the younger regions of the Pacific plate, but the directions diverge in the older regions (Nishimura and Forsyth, 1988). An anisotropic fast axis parallel to absolute plate motion may be indicative of shear flow at the base of the rigid oceanic lithosphere. A fast axis parallel to the fossil seafloor spreading direction may be indicative of azimuthal anisotropy frozen within the oceanic lithosphere at its formation. There are few previous seismic studies that focus on the Nova–Canton Trough, which is thought to be a relict of a major plate reorganization in the mid-Cretaceous (Joseph et al., 1993). The first Fresnel zone of the PS wave averages over strong variations in fossil spreading direction. In oceanic lithosphere formed before the mid-Cretaceous Long Normal magnetic chron, the fossil spreading direction between the Pacific and Phoenix plates is oriented N160°E (Larson et al., 1972). Joseph et al. (1993) concluded that the Nova–Canton Trough is the Middle Cretaceous extension of the Clipperton Fracture Zone, which suggests a 90° rotation of the fossil spreading direction early in the Long Normal chron, to N70°E. Sidescan-sonar and bathymetery data in the Nova–Canton Trough region reveal N140°E-striking abyssal hill topography south of the N70°E-striking structures of the Nova–Canton Trough and crustal fabric striking normal to the trough (N160°E) to the north (Joseph et al., 1993). These orientations agree poorly with the fast axis at N104.2°E that we infer from PS splitting data. A lateral average of fossil spreading could in principle lead to the orientation we observe, but the large delay times in the data make this explanation unlikely. Our results at the Nova–Canton Trough show that the anisotropic orientation from PS measurements appears more similar to the present-day absolute plate motion, roughly N110°E (Nishimura and Forsyth, 1988; Atwater and Sveringhaus, 1989). Based on this reasoning, we conclude tentatively that azimuthal anisotropy exists in the shear zone below the Pacific plate in the Nova–Canton Trough region.

A caveat arises if two anisotropic layers with distinct fast azimuths are present. For such a case the shear-wave splitting varies with the propaga-

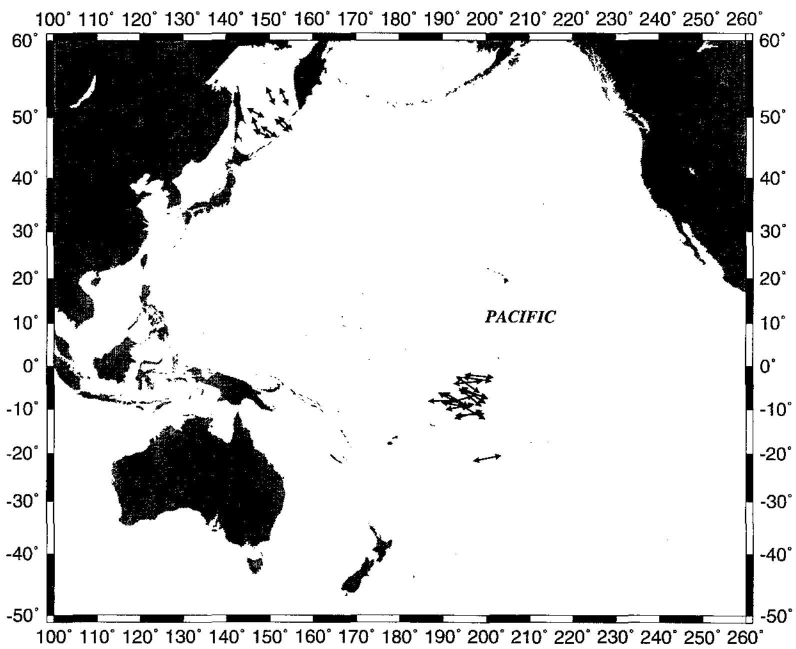

Fig. 9. Map of PS splitting results. The orientation of line segments indicates the inferred fast axis azimuth, but the delay time is not indicated graphically.

tion azimuth of the body wave, so that observations in a narrow azimuth range, as in this study, may not represent a simple vertical average of material properties (Savage and Silver, 1993). However, a plausible model for such a two-layer structure is fossil anisotropy in a shallow rigid lithosphere underlain by 'active' anisotropy in a sheared asthenosphere. Therefore, this caveat may not threaten our conjecture that the latter process is important in this part of the central Pacific.

The Kuril Islands region is structurally and dynamically complicated. Fischer and Yang (1994) used sS–S phase pairs to investigate the anisotropic structure in this region. They argued that olivine lattice-preferred orientation arises from four distinct strain regimes: shearing in the mantle wedge sub-parallel to the downgoing Pacific plate, compression of the upper plate beneath Kamchatka, extension in the Kuril Basin from Tertiary back-arc spreading, and ancient tectonism in the Eurasian continental lithosphere. In this study, the bounce points of PS lie to the north of the Kuril Islands within the Sea of Okhotsk, and are centered in the Kuril Basin area. The measurements of anisotropic orientation from PS waves are consistent with those of the sS–S phase pairs reported by Fischer and Yang. The agreement of the orientations of these two studies in the Kuril Basin region may imply that the tectonism of the Eurasian plate is a plausible mechanism to generate the upper-mantle anisotropy in this region. Alternatively, the orientation of the fast axis is consistent with shear strain associated with the absolute motion of the subducting slab.

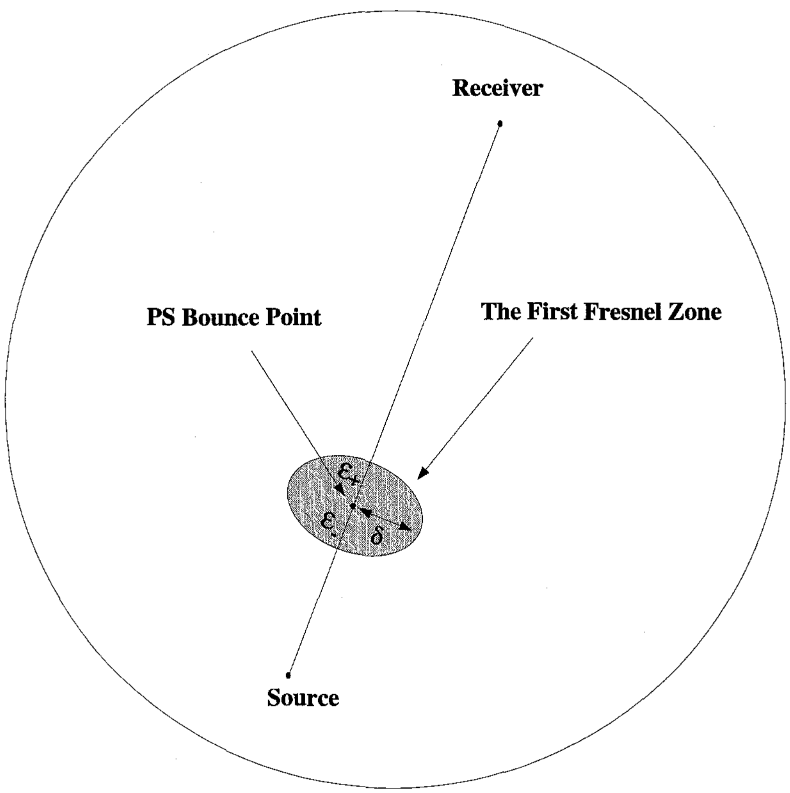

Fig. 10. Scheme to show the shape of the first Fresnel zone of the PS phase. In a typical case, which the epicentral distance is 110° and the source at 450 km with frequency 60 mHz (period approximately 17 s), $\epsilon^- = 3.2°$, $\epsilon^+ = 3.3°$, and $\delta = 3.6°$.

4.1. Conclusions: The utility of PS splitting

PS-Wave splitting is a promising method for investigating the anisotropic structure of regions remote from both seismicity and seismic stations. The easiest application of the observable is limited by the requirements of (1) deep earthquakes, (2) a restricted range in epicentral distance, and (3) weak shear-wave splitting beneath the receiver. The first and last of these desiderata can be relaxed somewhat. The PS and SP phases with periods of 5–10 s can be separated for intermediate-depth earthquakes. The restriction of our study to deep-focus events was made to allow unambiguous identification of the phases, and also for easier comparison with synthetic seismograms at longer period. If shear-wave splitting is generated beneath a receiver location, its effect on the PS phase can be subtracted before estimating the splitting associated with the bounce-point location.

For shallow events, PS and SP coincide. However, neither the PS nor the SP phase has displacement on the transverse component for an isotropic and spherically symmetric Earth. Thus, if we detect anomalous energy on the transverse component at the time of simultaneous PS and SP arrival, at least three possibilities arise. One possibility is the PS splitting discussed in this paper. Another possibility is that the P wave of SP is tilted to some angle by lateral and/or anisotropic structure near the receiver. This is consistent with the SP phase in some records in our study (e.g. Figs. 7 and 8), where the largely rectilinear motion of the SP phase argues against splitting and/or timing problems. Alternatively, if the shear wave of the SP suffers splitting before conversion to P, the transverse component displacement may arise from multipathed off-azimuth P phases. Some combination of these effects is plausible, as transverse-component anomalies can be associated with both PS and SP phases in our coupled-mode synthetic seismograms (Figs. 2 and 3). Further synthetic seismogram experiments at shorter period are necessary to assess these effects. The bounce points of SP and PS are widely separated on the source–receiver great circle, so that different upper-mantle regions are sampled. It is more difficult to analyze data from shallow events because of the coincident arrival of SP and PS, but it may be possible to use PS splitting from such data to probe anisotropy in remote regions.

Acknowledgments

Yang Yu, Neil Ribe, Phil Ihinger and Paul Silver made useful comments on the manuscript. George Helffrich reviewed the manuscript and made comments that improved the manuscript. This work was supported by NSF grant EAR-9219367, partly while J. Park was enjoying sabbatical leave at the Department of Terrestrial Magnetism, Carnegie Institute of Washington.

References

Ando, M. and Ishikawa, Y., 1982. Observations of shear-wave velocity polarization anisotropy beneath Honshu, Japan: two masses with different polarization in the upper mantle. J. Phys. Earth, 30: 191–199.

Atwater, T. and Sveringhaus, J., 1989. Tectonic maps of the northeast Pacific. In: (E.L. Winterer, D.M. Hussong and R.W. Decker (Editors), The Geology of North America, Vol. Geol. Soc. Am., Boulder, CO.

Dziewonski, A.M., Hales, A.L. and Lapwood, E.R., 1975. Parametrically simple earth models consistent with geophysical data, Phys. Earth Planet. Inter., 10: 12–48.

Eaton, D.W.S., Stewart, R.R. and Harrison M.P., 1991. The Fresnel zone for P–SV waves, Geophysics, 56: 360–364.

Fischer, K.M. and Yang, X., 1994. Anisotropy in Kuril–Kamchatka subduction zone structure. Geophys. Res. Lett., 21: 5–8.

Forsyth, D.W., 1975. The early structural evolution and anisotropy of the oceanic upper mantle, Geophys. J. R. Astron. Soc., 43: 103–162.

Hess, H.H., 1964. Seismic anisotropy of the uppermost mantle under oceans. Nature, 203: 629–631.

Joseph, D., Taylor, B., Shor, A.N. and Yamazaki, T., 1993. The Nova–Canton trough and the late Cretaceous evolution of the central Pacific. Geophys. Monogr. Am. Geophys. Union, 77: 171–185.

Kaneshima, S. and Silver, P.G., 1992. A search for source-side mantle anisotropy. Geophys. Res. Lett., 19: 1049–1052.

Keen, C.E. and Barrett, D.L., 1971. A measurement of seismic anisotropy in the northeast Pacific. Can. J. Earth Sci., 8: 1056–1076.

Keith, C.M. and Crampin, S., 1977. Seismic body waves in anisotropic media: synthetic seismograms, Geophys. J. R. Astron. Soc., 49: 225–243.

Kind, R., Kosarev, G.L., Makeyeva, L.I. and Vinnik, L.P., 1985. Observations of laterally inhomogeneous anisotropy in the continental lithosphere. Nature, 318: 358–361.

Larson, R.L., Smith, S.M. and Chase, C.G., 1972. Magnetic lineations of Early Cretaceous age in the western equatorial Pacific Ocean. Earth Planet. Sci. Lett. 15: 315–319.

Montagner, J.-P. and Tanimoto, T., 1990. Global anisotropy in the upper mantle inferred from the regionalization of phase velocities. J. Geophys. Res., 95: 4797–4819.

Nataf, H.-C., Nakanishi, I. and Anderson, D.L., 1984. Anisotropy and shear-velocity heterogeneities in the upper mantle. Geophys. Res. Lett., 11: 109–112.

Nicolas, A. and Christensen, N.I., 1987. Formation of anisotropy in upper mantle peridotites — a review. In: K. Fuchs and C. Froidevaux (Editors), Composition, Structure and Dynamics of the Lithosphere–Asthenosphere System, Vol. 16, pp. 111–123.

Nishimura, C.E. and Forsyth, D.W., 1988. Rayleigh wave phase velocities in the Pacific with implications for azimuthal anisotropy and lateral heterogeneities. Geophys. J. R. Astron. Soc., 94: 479–501.

Park, J. and Yu, Y., 1992. Anisotropy and coupled free oscillations: simplified models and surface wave observations. Geophys. J. Int., 110: 401–420.

Park, J. and Yu, Y., 1993. Seismic determination of elastic anisotropy and mantle flow. Science, 261: 1159–1162.

Raitt, R.W., Shor, G.G., Francis, T.J.G. and Morris, G.B., 1969. Anisotropy of the Pacific upper mantle. J. Geophys. Res., 74: 3095–3109.

Ribe, N.M., 1989a. A continuum theory for lattice preferred orientation. Geophys. J., 97: 199–207.

Ribe, N.M., 1989b. Seismic anisotropy and mantle flow. J. Geophys. Res., 94: 4213–4223.

Ribe, N.M. and Yu, Y., 1991. A theory for plastic deformation and textural evolution of olivine polycrystals. J. Geophys. Res., 96: 8325–8336.

Savage, M.K. and Silver, P.G., 1993. Mantle deformation and tectonics: constraints from seismic anisotropy in the western United States. Phys. Earth Planet. Inter., 78: 207–227.

Savage, M.K., Silver, P.G. and Meyer, R.R., 1990. Observations of teleseismic shear-wave splitting in the Basin and Range from portable permanent stations. Geophys. Res. Lett., 17:21–24.

Silver, P. and Chan, W.W., 1988. Implications for continental structure and evolution from seismic anisotropy. Nature, 335 (1 September): 34–39.

Silver, P. and Chan, W.W., 1991. Shear wave splitting and subcontinental mantle deformation. J. Geophys. Res., 96: 16429–16454.

Silver, P.G., Kaneshima, S. and Meade, C., 1993. Why is the lower mantle so isotropic? (abstract) EOS Trans. Am. Geophys. Union, Spring Mtg. Suppl., 74: 313.

Su, L., Park, J. and Yu, Y., 1993. Born seismograms using coupled free oscillations: the effects of strong coupling and anisotropy. Geophys. J. Int., 115: 849–862.

Tanimoto, T. and Anderson, D.L., 1985. Lateral heterogeneity and azimuthal anisotropy of the upper mantle: Love and Rayleigh waves 100–250 s. J. Geophys. Res., 90: 1842–1858.

Vinnik, L.P., Kosarev, G.L. and Makeyeva, L.I., 1984. Anizotropiya litosfery po nablyudeniyam voln SKS and SKKS. Dokl. Akad. Nauk SSSR, 278: 1335–1339.

Vinnik, L.P., Farra, V. and Romanowicz, B., 1989. Azimuthal anisotropy in the Earth from observations of SKS at GEOSCOPE and NARS broadband stations. Bull. Seismol. Soc. Am., 79: 1542–1558.

Yu, Y. and Park, J., 1993. Upper mantle anisotropy and coupled-mode long-period surface waves. Geophys. J. Int., 114: 473–489.

Yu, Y. and Park, J., 1994. Hunting for upper mantle anisotropy beneath the Pacific Ocean region. J. Geophys. Res., submitted.